

Are Au nanoparticles on oxygen-free supports catalytically active?

Alexander Yu. Klyushin¹, Rosa Arrigo¹, Yi Youngmi¹, Zilal Xie¹, Michael Hävecker^{1,2},
Andrey V. Bukhtiyarov^{3,4}, Igor P. Prosvirin^{3,4}, Valerii I. Bukhtiyarov^{3,4}, Axel Knop-
Gericke¹ and Robert Schlögl¹.

¹ Fritz-Haber-Institute der Max Planck Society, Faradayweg 4-6, 14195, Berlin, Germany

² Division Solar Energy Research, Helmholtz-Zentrum Berlin für Materialien und Energie GmbH, Albert-Einstein-Str. 15, 12489 Berlin, Germany

³ Borekov Institute of Catalysis, pr. Lavrentieva 5, Novosibirsk, 630090, Russia

⁴ Novosibirsk State University, Piragova str. 2, Novosibirsk, 630090, Russia

Abstract:

Gold nanoparticles (Au NPs) on oxygen-free supports were examined using near ambient pressure X-ray photoelectron spectroscopy (NAP-XPS) under CO oxidation conditions, and *ex-situ* using scanning electron microscopy (SEM) and transmission electron microscopy (TEM). Our observations demonstrate that Au NPs supported on carbon materials are inactive, regardless of the preparation method. Ozone (O₃) treatment of carbon supports leads oxygen-functionalization of the supports. When subsequently exposed to a CO feed, CO is oxidized by the functionalized sites of the carbon support via a stoichiometric pathway. Microscopy reveals that the reaction with CO does not change the morphology of the Au NPs. *In-situ* XPS reveals that the O₃ treatment gives rise to additional Au 4f and O 1s peaks at binding energies of 85.25-85.6 eV and 529.4-530 eV, respectively, which are assigned to the presence of Au oxide. A surface oxide phase is formed during the activation of Au NPs supported on Au foil by O₃ treatment. However, this phase decomposes in vacuum and the remaining low-coordinative atoms do not have sufficient catalytic properties to oxidize CO, so the size reduction of Au NPs and/or oxidation of Au NPs is not sufficient to activate Au.

Keywords: Gold nanoparticles, gold oxide, X-ray photoemission spectra, surface core-level shift, CO oxidation, strong metal-support interaction.

1. INTRODUCTION

Gold-based catalysts have attracted a lot of interest since Haruta's study [1,2]. Au catalytic systems demonstrate high activity in many application, in particular in complete [3,4], selective [5,6] and partial [3,7] oxidation reactions. The number of publications on the application of Au in catalysis increases each year; however, the mechanism of the reactions is still debated in the literature.

The complexity of Au-containing catalysts suggests many possible factors may influence the catalytic activity of gold, such as particle size and shape, the support morphology and nature, activation (pre-)treatment, presence of adsorbed oxygen or water etc. In the literature, there is no consensus about active species; some authors consider metallic gold [8,9] as active sites, while others suggest positive (δ^+) [10,11] and negative (δ^-) [12,13] low-charged gold or oxidized ($1^+,3^+$) states [14]. Identification of active sites requires a systematic study of Au-based catalysts, by varying one or few parameters. One of the potentially most important parameters is the support. Therefore we divide Au catalytic systems into two broad groups: Au on oxygen-free supports and Au on oxides.

Here, we present a study of Au catalysts on oxygen-free supports in the CO oxidation reaction, using a combination of *in-situ* XPS and *ex-situ* TEM and SEM. NAP-XPS measurements allow us to characterize the electronic structure of nanoscopic Au and support, while microscopy provides information about morphology of Au NPs before and after reaction. The combination of these techniques helps one to understand the origin of Au catalytic activity and clarify the mechanism of the reaction.

2. MATERIALS

2.1 Au/HOPG

Model Au/HOPG catalysts were prepared inside a preparation chamber attached to a photoelectron spectrometer (Novosibirsk, Russia) which was built by SPECS (Germany). The analyzer chamber was equipped with a hemispherical analyzer PHOIBOS-150-MCD-9, an ellipsoidal monochromator FOCUS 500 and an X-ray source XR 50 M with double Al/Ag anode. The three-step preparation procedure, previously used to prepare Ag/HOPG (highly oriented pyrolytic graphite) model catalysts, as described in detail elsewhere [15], was used to prepare Au/HOPG model catalysts. This procedure consists of an initial stage of defect formation on the HOPG surface by soft Ar⁺ sputtering followed by Au deposition and surface annealing at T = 300 °C in UHV (for Au NPs stabilization). The Au nanoparticle size was varied by changing the amount of deposited gold, which was controlled by monitoring the ratio of Au 4f to C 1s XPS peak areas, a final Au load was 1 wt%.

2.2 Au/N-CNTs

Multi-walled carbon nanotubes were supplied by Applied Science Ltd. 20 g CNTs were treated with 1 L of concentrated HNO₃ under reflux for 4 h. Then the nanotubes were filtrated and washed with distilled water until the filtrate showed a neutral pH. Subsequently, the sample was dried at 110 °C for 3 d in air. N-functionalized CNTs (N-CNTs) were obtained via a treatment of the previously oxidized nanotubes with NH₃ at 700 °C for 6h. For this purpose 3g of the material were placed in a quartz tube under a flow of 120 ml/min composed of 10% NH₃ in Ar.

5 mg of NaN₃ were dissolved in 10 ml of MilliQ water. Then 6 mg of trihydrate chloroauric acid (HAuCl₄·3H₂O) were added to the solution, which subsequently turned orange. The ratio NaN₃/HAuCl₄·3H₂O was 5:1. 300 mg of N-CNTs were added to the solution in order to allow the adsorption of the Au precursor on the N-CNTs with a final Au load of 1wt%. The

addition of the N-CNTs induced gas release and caused the solution to turn colorless, indicating the decomposition and complete adsorption of the precursor. Afterwards, the N-CNT suspension was filtered and the total precursor decomposition was ensured by photo-treatment with an UV/Vis lamp for 30min.

2.3 Au/O-CNTs

10 g Baytubes C150HP were treated with 500 mL of 3 molar HNO₃ (diluted with water from nitric acid 65% (Merck)) at room temperature (RT) for 24 h. Then the O-functionalized CNTs (O-CNTs) were thoroughly washed and filtrated with Millipore water until a neutral pH was obtained. For the synthesis of Au/O-CNT, 1 g of O-CNTs was impregnated with 6 mL aqueous solution containing 20.2 mg of HAuCl₄. The slurry was then sonicated in an ultrasonic bath for 10 sec and afterwards the solvent was evaporated slowly at RT in air for 48h. Thereafter, the samples containing the metal precursor were reduced in 20% H₂/Ar gas mixture at 250 °C for 2h, a final Au load was 1 wt%.

2.4 Au/Au foil

Au nanoparticles on Au foil were prepared by electrodeposition. Electrochemical deposition was performed in a conventional three-electrode electrochemical cell using a potentiostat/galvanostat (VSP, Biologic). Au foil was used as the working electrode and Pt wire and saturated calomel electrode (SCE) were employed as the counter electrode and the reference electrode. Au electrolyte solution consisted of 0.1 mM HAuCl₄ + 0.1 M HCl. Au nanoparticles were then electrodeposited under a current potential of -0.4 V vs. SCE for 60 s.

3. METHODS

3.1 XPS

The NAP-XPS experiments were performed at the ISIS beamline of BESSY II/HZB (Berlin, Germany). All measurements were carried out in a stainless steel NAP-XPS chamber, the details of which are described elsewhere [16,17]. The powder samples were pressed into a

pellet of 8 mm diameter. Samples were placed between a stainless steel backplate and lid (with 6 mm hole) and mounted onto a sapphire sample holder. The samples were heated from the backside using an infrared laser and the temperature was measured by a thermocouple fastened to the sample surface. The overall spectral resolution was 0.3 eV in O 1s and 0.2 eV in Au 4f regions. The spectra intensity was normalized to the incident photon flux, which was measured using a Au foil. The core level binding energies (BE) were calibrated using the Fermi edge, C 1s and Au 4f_{7/2} second order peak. The accuracy of BE calibration was estimated to be around 0.05 eV.

All XP spectra were collected in normal photoemission mode. For quantitative XPS analysis, least-squares fitting of the spectra were performed using CasaXPS software (www.casaxps.com). A Doniach-Sunjic line shape for Au 4f_{7/2} and a product (multiplication) of a Gaussian with a Lorentzian line shape for O 1s with Shirley-type background were used to obtain the best fit. For surface composition calculation the cross section tables of Yeh and Lindau were used [18] and the correction for the different electron inelastic mean free pass was done using QUASES-IMFP-TPP2M software (<http://www.quases.com/products/quases-imfp-tpp2m/>).

O₃ was produced using a commercial ozone generator TC-1KC. Oxygen was flowed through Teflon tubing to the ozone generator at a rate of 1 L/min. The effluent gas of the generator contained a mixture of approximately 1% ozone and 99% un-reacted oxygen. The O₃/O₂ mix was dosed into the experimental cell using a leak valve. O₂ and CO were dosed into the experimental cell in different ratios using mass-flow controllers (MFC) at a sample temperature of 100 °C. The total pressure in the experimental cell was 0.3 mbar.

4. RESULTS

4.1 Au/HOPG.

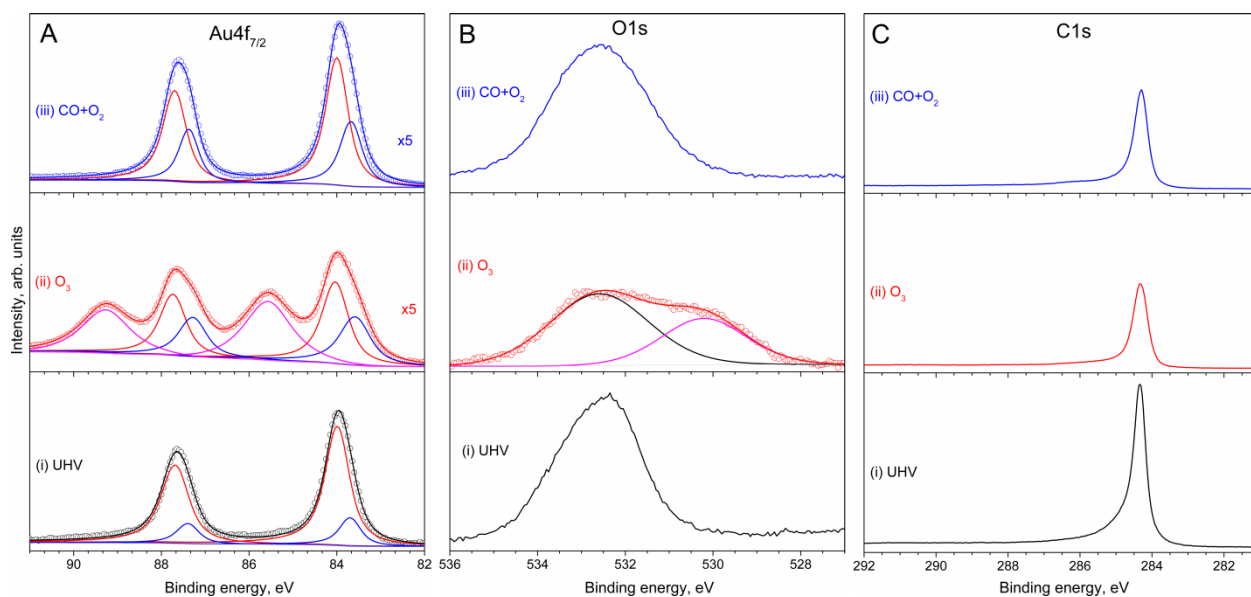


Figure 1. NAP (a) Au 4f, (b) O 1s and (c) C 1s XP spectra of Au/HOPG (i) in UHV at RT, (ii) under O₃ at p=0.3 mbar, T=100 °C and (iii) under CO and O₂ atmosphere at p=0.3 mbar, RT. Photoelectrons with 150 eV kinetic energy were used to collect surface sensitive Au 4f, O 1s and C 1s spectra in UHV and CO+O₂, and photons with 720 eV energy were used to collect Au 4f, O 1s and C 1s spectra during O₃ treatment.

The first step to study the Au catalyst is to characterize the freshly prepared samples. Photoelectrons with 150 eV kinetic energy were used to collect surface sensitive Au 4f, O 1s and C 1s spectra in UHV and CO+O₂, and photons with 720 eV energy were used to collect Au 4f, O 1s and C 1s spectra during O₃ treatment (Figure 1). Au 4f spectrum of the fresh Au/HOPG in UHV at RT (Figure 1A(i)) shows one sharp peak at a binding energy (BE) of 83.95 eV, assigned to bulk Au in the metallic state, according to the literature [19-21]. The component shifted to low BE by the 0.3 eV is usually assigned to low-coordinated Au atoms [22]. The corresponding O 1s spectrum shows the presence of oxygen on the surface (Figure 1B(i)). The asymmetry of O 1s peak indicates that there is more than just one oxygen specie and the position of its maximum

(BE 532.6 eV) suggests the presence of C-O, C=O and/or C-OH bonds [23,24]. C 1s spectrum (Figure 1C(i)) shows well-known graphite peak at BE of 284.3 eV [25].

When the O₂/O₃ mixture was introduced into the chamber and the sample was heated to 100 °C, the Au 4f spectrum changed (Figure 1A(ii)). A well-defined peak appears at 85.6 eV, which is assigned to an ionic Au species [21,26]; however, with lower BE than that of Au₂O₃ (BE 85.9 eV) [27,28]. Under O₃ the numbers of low coordinated Au atom increasing, this is evidenced by an increase and broadening in low BE peak at 83.5 eV. According to Weststrate et al. [22] the less neighbors the lower BE, in other words an oxidation restructures Au surface and forms low-coordinated Au atoms (for example edges, kinks, etc.) on the surface. The surface sensitive O 1s spectrum (Figure 3B(ii)) is broader in comparison with one measured in UHV. The O 1s spectrum in O₃ atmosphere consists of at least two components: the high BE species are associated with carbon-oxygen species (BE 532.6 eV) while the low BE component corresponds to oxygen on Au (BE 530.1 eV) [21,29]. A decrease in intensity of C 1s spectrum (Figure 1C(ii)) is due to scattering of photoelectron in gas phase.

As was shown in our previous work [30], all signs of gold oxide vanish when O₃ is evacuated from the chamber. Even an O₂-rich gas mixture (CO/O₂=1:75) does not prevent the decomposition of the oxide (Figure 1(iii)). In contrast to the changes found for extended Au surfaces exposed to ozone [30], the Au 4f spectral shape of Au NPs remains unchanged after O₃ treatment (Figure 1A(iii)). The low BE components of the Au 4f spectra does not change much, only small intensity decrease, which can be due to sintering or/and carbon accumulation (Figure 1C(iii)). Consistently, the peak shape of the O 1s spectrum returns to nearly the same shape as when measured in UHV, but with a slightly broader width due to the formation of new carbon-oxygen species. Note that only oxygen bonding to the carbon remains on the surface.

Table 1. Surface composition of Au/HOPG at different conditions.

| | Au ⁰ , at. % | Au ³⁺ , at. % | O, at. % | C, at. % |
|-------------------|-------------------------|--------------------------|----------|----------|
| UHV | 16.5 | - | 5.0 | 78.5 |
| O ₃ | 7.4 | 4.6 | 9.5 | 75.5 |
| CO+O ₂ | 8.0 | - | 10.3 | 81.7 |

The quantitative analysis of surface composition is presented in Table 1. The dominant element on the surface obviously is carbon at all conditions. The amount of Au on the untreated sample is 16.5 at. %. O₃ treatment leads to oxidation of ca. 30% of Au and significant increasing of oxygen concentration. Decreasing of Au concentration during and after O₃ treatment points out, that the sintering takes place.

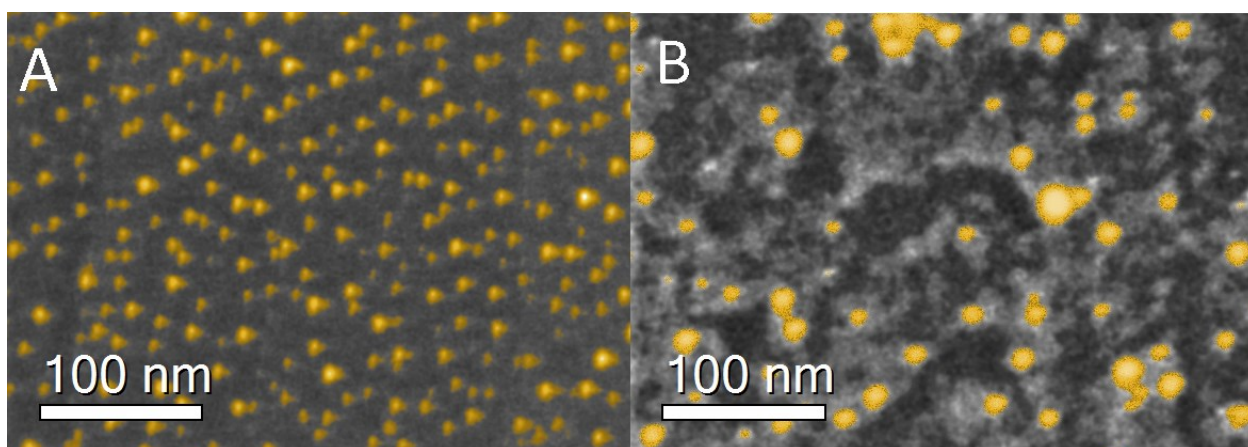


Figure 2. SEM image of Au/HOPG a) before and b) after O₃ treatment at 250 °C and CO oxidation. Images were colorized in order to highlight the differences between the two samples.

The structural evolution of Au NPs during CO oxidation may help to shed light on the origin of Au activation. An SEM image of the untreated Au/HOPG is presented in Figure 2A. The image shows Au NPs with a narrow size distribution of 6-8 nm. After O₃ treatment and CO oxidation, the Au NPs are not homogeneously distributed anymore, as shown in Figure 2B. The mean particle size is higher (~10 nm) than the fresh sample and some agglomerated particles are

visible, which is in good agreement with quantification of the surface composition made by XPS. Burning of graphite at the interface with the Au NPs is accompanied by the migration of metallic particles on the HOPG surface (the tracks are darker in Figure 2b). This may occur because the aggressive oxidation by O₃ leads to high mobility of Au NPs due to destruction (burning and oxidation) of carbon surface [31].

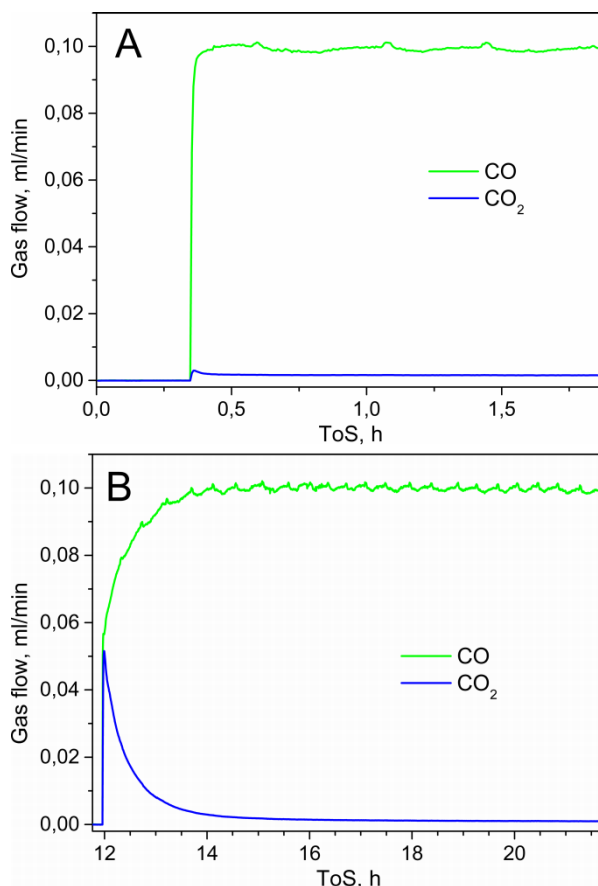


Figure 3. QMS data of Au/HOPG a) before and b) after O₃ treatment at p=0.3 mbar, RT and CO:O₂=1:75 ratio.

To estimate catalytic performance Au/HOPG sample was placed in the NAP-XPS chamber without any pretreatment. Then the reaction mixture (CO:O₂=1:75) was introduced to the chamber (Figure 3A). Small fluctuations of CO flow are due to fluctuations of the MFC at very low flow. Initially, the CO₂ yield exhibits a small increase for a short time: we attribute this

activity to a reaction between CO and residual O on the HOPG surface. For long time on stream, Au/HOPG does not show any significant activity under the described conditions, therefore we reason that nanostructuring is not sufficient to activate Au.

We tried to slightly oxidize Au before the reaction, using an O₃ treatment. QMS data is presented in Figure 3B, in which Au NPs that were pre-treated with O₃ are exposed to a constant flow of a 1:75 mixture of CO and O₂. The activity of the oxidized sample is much higher than that of the sample not pre-treated with O₃, but a strong deactivation takes place, and after approximately 2 hours the CO₂ yield is negligible. Thus the agglomeration does not influence the activity of Au/HOPG, suggesting that other reasons apart of the structural changes are responsible of the activation of Au. We assume that the increase of the CO₂ yield after the O₃ treatment is caused by the stoichiometric reaction between the remaining surface oxygen and CO.

4.2 Au/N-CNTs and Au/O-CNTs

Similar results were obtained for Au NPs on nitrogen- and oxygen-functionalized carbon nanotubes (Au/N-CNTs and Au/O-CNTs). The Au particle size was <5nm. The Au NPs on functionalized CNTs consisted of a few large (ca. 40 nm diameter) particles, sparsely distributed along the tubes (not shown), along with a majority of densely dispersed nanoclusters visible only by STEM (ESI, Fig. S1). Under the same conditions, the fresh samples were inactive for CO oxidation as Au/HOPG, in spite of the significant increase of the catalyst surface area that resulted from the higher support area and Au size reduction. After O₃ treatment, Au/N-CNTs and Au/O-CNTs show the same initial activity profile as discussed for Au/HOPG and, the same rate of deactivation (~2.5 hours) (not shown).

4.3 HOPG

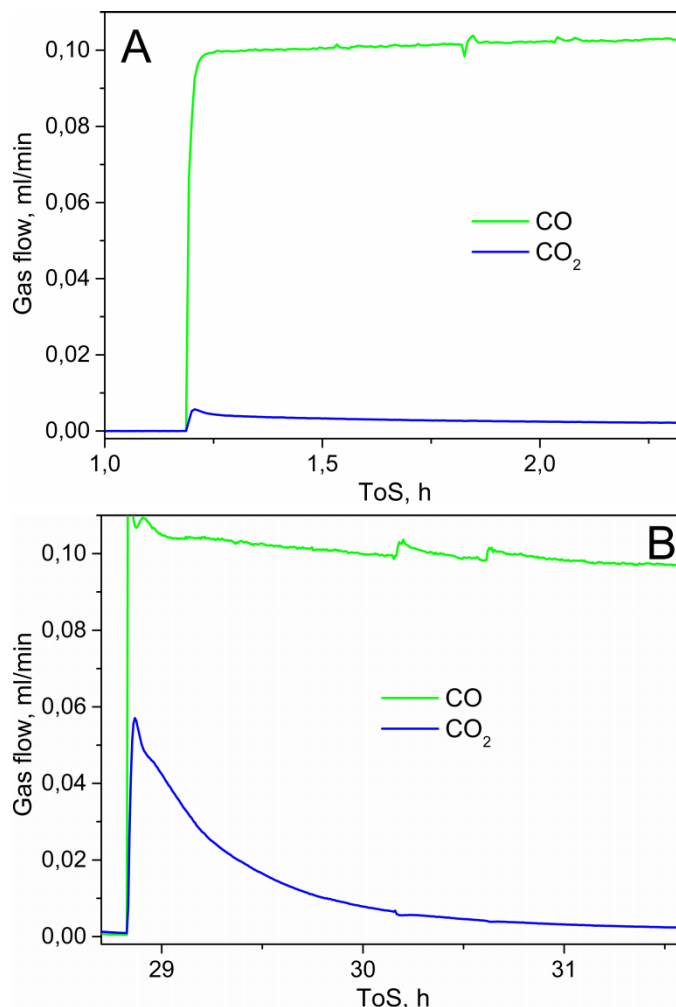


Figure 4. QMS data of HOPG a) before and b) after O₃ treatment at p=0.3 mbar, RT and CO:O₂=1:75 ratio.

In order to prove that stoichiometric reaction takes place, ‘blank’ measurements were done. A pristine HOPG crystal was placed in the sample holder and all treatment procedures were repeated. The QMS results are shown in the Figure 4. Untreated HOPG does not catalyze the oxidation of CO as clearly shown in the Figure 4A. However after interaction with O₃, HOPG demonstrates an initial high CO conversion that strongly decreases with time. Since HOPG contains only carbon atoms, the origin of sample’s activity can be attributed only to the

stoichiometric reaction between chemisorbed oxygen on the HOPG surface and CO in the gas phase.

4.4 Au/Au foil

To further corroborate the idea that the reactivity is due to a stoichiometric reaction between CO and O functional groups on the carbon surface, we investigated Au nanoparticles supported on oxygen-free Au foil. The Au foil was chosen as a support because it is expected to be inactive in CO oxidation.

After preparation, the surface composition of the Au/Au foil is very important. All fitting parameters are given in Tables S1 and S2 in the ESI. The corresponding Au 4f spectrum (Figure 5A(i)) of Au/Au foil shows the metallic peak at a BE of 83.95 eV with second component shifted to the low BE by 0.3 eV. This peak is assigned to the surface core-level shift [32,33], which is ascribed mainly to the lower coordination of surface atoms compared to bulk atoms. The O 1s spectrum (Figure 5B(i)) displays one broad peak at BE of 532.5 eV, which is in the range observed for carbonates and oxygen-containing (hydro)carbons on gold [34]. The presence of carbonates and/or oxygen-containing (hydro)carbons on the surface is confirmed by the C 1s spectrum (Figure 5C(i)).

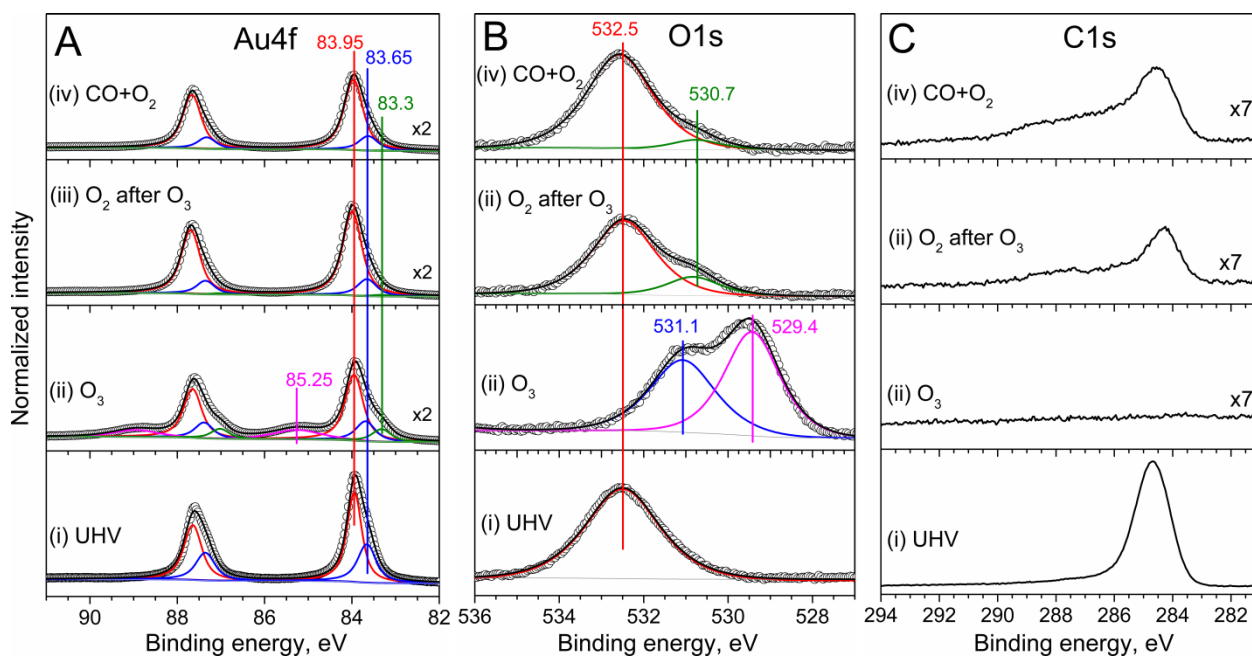


Figure 5. NAP (a) Au 4f, (b) O 1s and (c) C 1s XP spectra of Au/Au foil (i) in UHV at RT, (ii) under O₃ at p=0.3 mbar, T=150 °C, (iii) under O₂ after O₃ treatment at p=0.3 mbar, RT and (iv) under CO and O₂ atmosphere (CO:O₂=1:75) at p=0.3 mbar, RT. Photoelectrons with 150 eV kinetic energy were used to collect surface sensitive Au 4f, O 1s and C 1s spectra in UHV, and photons with 720 eV energy were used to collect Au 4f, O 1s and C 1s spectra in O₃, O₂ and CO+O₂ atmospheres.

To clean the Au surface from the surface carbon impurities, an O₃ treatment at 150 °C was performed. When we apply the combination of high temperature (150 °C) and very reactive treatment (O₃) the carbon is burned of very rapidly, as is clearly visible in the Figure 5C(ii). The influence of the O₃ to the sample is not limited only to the burning of the carbon, but also the oxidation of the Au surface takes place. The corresponding Au 4f spectrum (Figure 5A(ii)) reveals the formation of Au oxide, the broad peak at BE of 85.25 eV appears under O₃ conditions, which is assigned to an ionic Au species [21,26]. Simultaneously, a new feature in comparison with the untreated sample appears in low BE region (BE=83.3 eV), which is

assigned to the surface restructuring during oxidation [30,35]. The O 1s spectrum (Figure 5B(ii)) has also undergone changes: the broad peak at 532.5 eV vanishes due to carbon removal and a double peak in the lower BE region is formed. The component with BE of 529.4 eV can be assigned to a surface oxide or chemisorbed oxygen on Au [29,36,37]; the other component (BE=531.1 eV) has to be attributed to O in water and/or hydroxyl groups [21,29], but also the oxidation of contaminants in concentrations below the detection limits of XPS cannot be excluded [29].

After O₃ cleaning the sample was cooled down to RT and O₃ was substituted by O₂. The cooling leads to immediate carbon accumulation as shown in the C 1s spectrum (Figure 5C(iii)). The high BE tail of the C 1s spectrum indicates the formation of C-O and C=O bonds on the surface during cooling in O₃ and further treatment in O₂. The O 1s spectrum in O₂ (Figure 5B(iii)) confirms the formation of oxygen-containing (hydro)carbons on the Au surface, corresponding peak at 532.5 eV is well pronounced. In addition a small peak at 530.7 eV arises, and can be assigned to residual oxidized impurities in concentrations below XPS detection limit or to (hydro)carbons adsorbed on the low-coordinated atoms (defects) on the surface. There is no peak (BE <530 eV) related to the Au oxide(s). Also no signs of Au oxide(s) (BE 85.25 eV) are in the Au 4f spectrum (Figure 5A(iii)), but deconvolution of the spectrum shows that the peak assigned to the surface reconstruction (BE 83.3 eV) remains. Therefore, O₃ evacuation leads to decomposition of oxide(s) and carbon accumulation.

Following O₃ treatment, we introduced a reaction mixture (CO/O₂=1:75) into the chamber. The spectra do not change substantially. Further carbon accumulation occurs, as is seen by the increase in intensity of the C 1s peak (Figure 5C(iv)). The shapes of the O 1s (Figure 5B(iv)) and Au 4f (Figure 5A(iv)) spectra are similar in general to the ones measured in O₂ atmosphere; only the intensity of the peak (BE=530.7 eV) corresponding to residual residual oxidized impurities

with concentrations below XPS detection limit or to (hydro)carbons adsorbed on the low-coordinated atoms (defects) decreases.

Table 2. Surface composition of Au/Au foil at different conditions.

| | Au⁰, at. % | Au³⁺, at. % | O, at. % | C, at. % |
|-------------------|------------------------------|-------------------------------|-----------------|-----------------|
| UHV | 24.8 | - | 6.2 | 69.0 |
| O ₃ | 47.7 | 8.9 | 41.8 | <1.5 |
| O ₂ | 37.3 | - | 23.4 | 39.3 |
| CO+O ₂ | 8 | - | 10.3 | 81.7 |

Quantification of the surface composition of Au/Au foil is presented in Table 2. The untreated sample is mostly covered by carbon (69.0 at. %). Nevertheless initial considerable carbon coverage O₃ treatment cleans surface from carbon totally. Contemporaneously to carbon burning Au oxidation takes place during O₃ treatment, oxygen concentration on the surface in O₃ atmosphere exceeds stoichiometric ratio of Au₂O₃, which indicates the presence of an additional adsorbed oxygen overlayer. Changing chemical potential from O₃ to O₂ leads the decomposition of the surface oxide and fast carbon accumulation (39.3 at. %); carbon comes from the wall of the chamber. Following CO oxidation only facilitates further increasing carbon concentration on the surface of Au/Au foil.

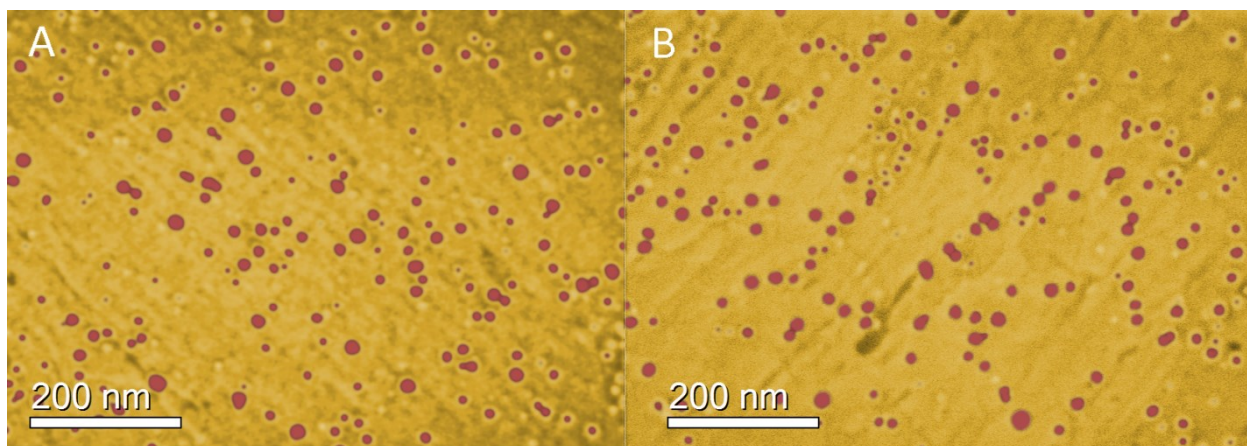


Figure 6. SEM images of Au/Au foil a) before and b) after O₃ treatment. Images were colorized in order to highlight the differences between the two samples.

Microscopy does not reveal big differences between fresh and oxidized samples. SEM images of untreated Au/Au foils show a particle size of ca. 10 nm (Figure 6A). In turn, the Au particle size distribution on O₃-treated samples shows some sintering effects and a slightly rougher surface (Figure 6B).

A fresh electrochemically prepared sample Au/Au foil was tested under reaction conditions (Figure 7A). The presence of the sample in the set-up does not influence the CO conversion. The CO₂ yield is negligible for the overall measurements. There are two possible explanation: 1) the adsorption of (hydro)carbons (See XPS part), which cover the surface, may prevent access of the gas mixture to the catalyst surface; or 2) Au/Au foil is an inactive catalyst. Our experiments with Au NPs (~15 nm) supported on transition metal oxides (Au/TiO₂ and Au/Fe₂O₃) in CO oxidation conducted under similar conditions show catalytic activity of the samples despite a big particle size and the presence of carbon on the surface up to 60 at. % [38], therefore surface (hydro)carbons are not relevant for inertness of Au NPs on oxygen-free supports.

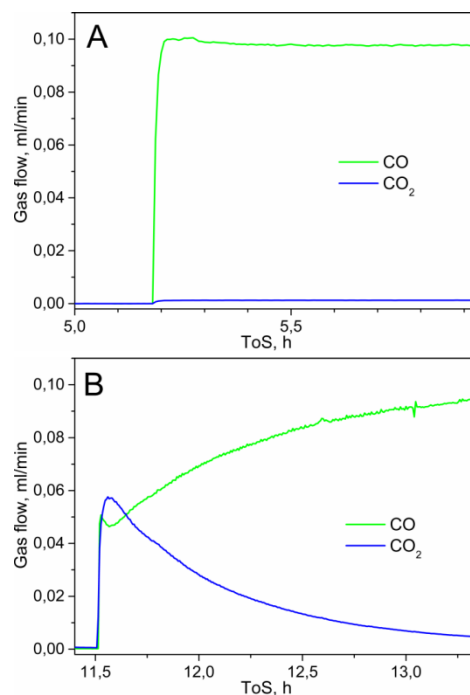


Figure 7. QMS data of Au/Au foil a) before and b) after O₃ treatment at p=0.3 mbar, RT and CO:O₂=1:2 ratio.

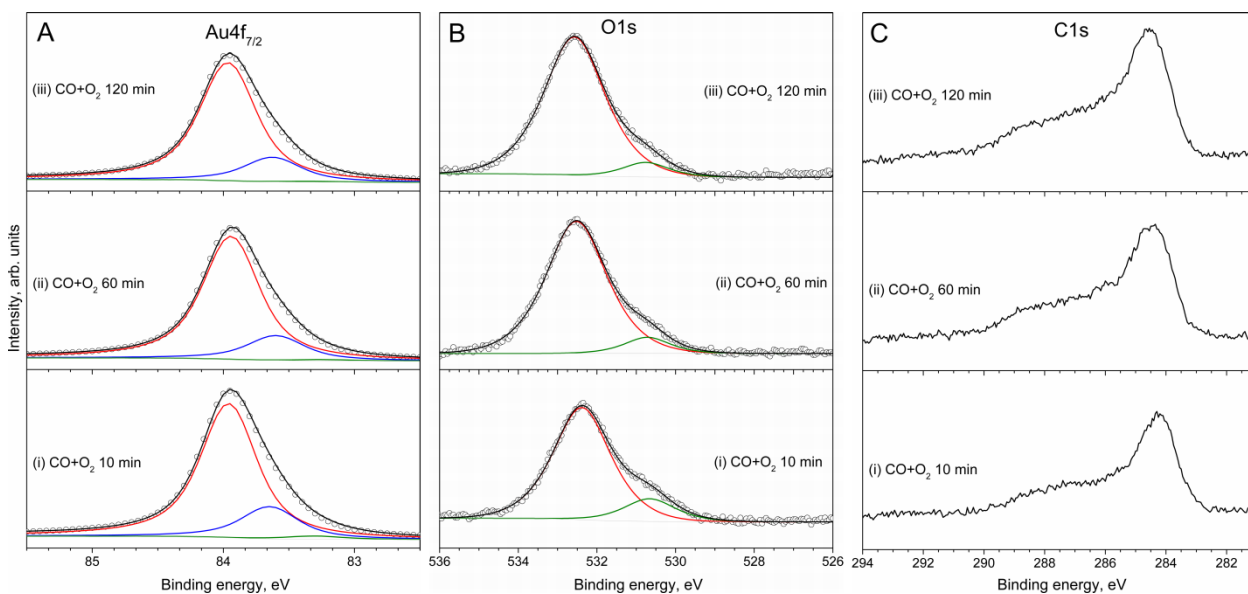


Figure 8. NAP (a) Au 4f, (b) O 1s and (c) C 1s XP spectra of Au/Au foil under CO reaction after O₃ treatment at p=0.3 mbar, RT (i) after 10 min, (ii) 60 min and (iii) 120 min. Photons with 720 eV energy were used to collect Au 4f, O 1s and C 1s spectra.

However, the oxidized Au sample looks more promising, but is not stable for long times (Figure 7B). CO consumption and deactivation time (2 hours) are similar to those observed on

Au/HOPG. The corresponding Au 4f, O 1s and C 1s spectra are shown in Figure 8. In the Au 4f spectrum (Figure 8A) the peak assigned to surface reconstruction (BE 83.3 eV) is present in a small amount. The overall intensity of the spectra decreases with time. The two components of the O 1s spectra (Figure 8B) show opposite behavior: the oxygen-containing (hydro)carbons (BE=532.5 eV) peak increases, while the intensity of the peak (BE=530.7 eV) corresponding to residual oxidized contaminants with concentrations below XPS detection limit or to (hydro)carbons adsorbed on the low-coordinated atoms (defects) decreases during the reaction. The explanation of such behavior can be that the reaction occurs between oxidized (hydro)carbons (O_3 functionalized carbon all over the chamber) and CO molecules. When the oxygen supply is depleted the reaction stops, and carbon accumulation takes place, which is evident from increasing of C 1s peak (Figure 8C). Thus, oxidized Au/Au foil itself does not catalyze CO oxidation at low temperature.

CONCLUSIONS

The results presented here indicate that Au NPs supported on oxygen-free substrates are not active catalysts in CO oxidation, unless an external source of oxygen is provided. This behavior is found to be independent of the method of preparation and the nature of the support. O_3 treatment allows cleaning of the surface, but at the same time to functionalize the carbon all over the chamber including the support. Oxygen-functionalized (hydro)carbon may still be present if their removal by O_3 treatment was not completed, and can react with CO. The stoichiometric reaction ends rather soon after reaction initiation, and O_2 alone cannot re-functionalize the (hydro)carbons.

Under a constant chemical potential of O_3 , an Au oxide is formed, but evacuation or substitution of O_3 by O_2 results in the disappearance of the surface oxide. Therefore, participation of Au oxide in CO oxidation can be excluded. Remaining low-coordinated atoms

do not have sufficient catalytic properties, and CO oxidation does not occur on the Au NPs even after oxidation. Our results clearly show that the size reduction and/or the oxidation of Au is not an effective strategy to activate Au.

ACKNOWLEDGMENT

We thank HZB for the allocation of synchrotron radiation beamtime, Gisela Weinberg (Fritz-Haber-Institute der Max-Planck, Berlin) for the SEM characterization, Manfred Schuster (Fritz-Haber-Institute der Max-Planck, Berlin) and Xing Huang (Fritz-Haber-Institute der Max-Planck, Berlin) for the TEM images and Klaus Friedel (Fritz-Haber-Institute der Max-Planck, Berlin) for sample preparation.

Grant of President of Russian Federation for government support of Leading Scientific Schools (grant SS-5340.2014.3).

REFERENCES

1. Haruta M., Yamada N., Kobayashi T., Iijima S. (1989) *J. Catal.* 115: 301-309.
2. Haruta M., Tsubota S., Kobayashi T., Kageyama H., Genet M.J., Delmon B. (1993) *J. Catal.* 144: 175-192.
3. Haruta M., Daté M. (2001) *Appl. Catal. A Gen.* 222: 427-437.
4. Hashmi A.S.K., Hutchings G.J. (2006) *Angew. Chem. Int. Ed.* 45: 7896-7936.
5. Laguna O.H., Romero-Sarria F., Centeno M.A., Odriozola J.A. (2010) *J. Catal.* 276: 360-370.
6. Ryabenkova Y., He Q., Miedziak P.J., Dummer N.F., Taylor S.H., Carley A.F., Morgan D.J., Dimitratos N., Willock D.J., Bethell D., Knight D.W., Chadwick D., Kiely C.J., Hutchings G.J. (2013) *Catal. Today.* 203: 139-145.
7. Hayashi T., Tanaka K., Haruta M. (1998) *J. Catal.* 178: 566-575.

8. Tripathi A.K., Kamble V.S., Gupta N.M. (1999) *J. Catal.* 187: 332-342.
9. Bär T., Visart de Bocarmé T., Nieuwenhuys B.E., Kruse N. (2001) *Catal. Letters.* 74: 127-131.
10. Guillemot D., Borovkov V.Yu., Kazansky V.B., Polisset-Thfoin M., Fraissard J. (1997) *J. Chem. Soc. Faraday Trans.* 93: 3587-3591.
11. Boccuzzi F., Chiorino A., Manzoli M., Lu P., Akita T., Ichikawa S., Haruta M. (2001) *J. Catal.* 202: 256-267.
12. Chen M.S., Goodman D.W. (2004) *Science* 306: 252-255.
13. Yoon B., Häkkinen H., Landman U., Wörz A.S., Antonietti J.-M., Abbet S., Judai K., Heiz U. (2005) *Science* 307: 403-407.
14. Minicò S., Scirè S., Crisafulli C., Visco A.M., Galvagno S. (1997) *Catal. Letters.* 47: 273-276.
15. Demidov D.V., Prosvirin I.P., Sorokin A.M., Rocha T., Knop-Gericke A., Bukhtiyarov V.I. (2011) *Catal. Sci. Technol.* 1: 1432-1439.
16. Knop-Gericke A., Kleimenov E., Hävecker M., Blume R., Teschner D., Zafeiratos S., Schlögl R., Bukhtiyarov V.I., Kaichev V.V., Prosvirin I.P., Nizovskii A.I., Bluhm H., Barinov A., Dudin P., Kiskinova M. (2009) *Adv. Catal.* 52: 213-272.
17. Bluhm H., Hävecker M., Knop-Gericke A., Kleimenov E., Schlögl R., Teschner D., Bukhtiyarov V.I., Ogletree D.F., Salmeron M. (2004) *J. Phys. Chem. B* 108: 14340-14347.
18. Yeh J.J., Lindau I. (1985) *At. Data Nucl. Data Tables* 32: 1-155.
19. Canning, N.D.S., Outka D., Madix R.J. (1984) *Surf. Sci.* 141: 240-254.
20. King D.E. (1995) *J. Vac. Sci. Technol. A* 13: 1247-1253.
21. Koslowski B., Boyen H.-G., Wilderotter C., Kästle G., Ziemann P., Wahrenberg R., Oelhafen P. (2001) *Surf. Sci.* 475: 1-10.

22. Weststrate C.J., Lundgren E., Andersen J.N., Rienks E.D.L., Gluhoi A.C., Bakker J.W., Groot I.M.N., Nieuwenhuys B.E. (2009) *Surf. Sci.*, 603: 2152–2157.
23. Desimoni E., Casella G.I., Morone A., Salvi A.M. (1990) *Surf. Interface Anal.* 15: 627-634.
24. Kundu S., Wang Y., Xia W., Muhler M. (2008) *J. Phys. Chem. C* 112: 16869–16878.
25. Witek G., Noeske M., Mestl G., Shaikhutdinov S., Behm R.J. (1996) *Catal. Lett.* 37: 35-39.
26. Tsai H., Hu E., Perng K., Chen M., Wu J.-C., Chang Y.-S. (2003) *Surf. Sci.* 537: L447–L450.
27. Juodkazis K., Juodkazyte J., Jasulaitiene V., Lukinskas A., Sebeka B. (2000) *Electrochem. Commun.* 2: 503–507.
28. Dickinson T., Povey A.F., Sherwood P.M.A. (1975) *J. Chem. Soc. Faraday Trans.* 71: 298-311.
29. Krozer A., Rodahl M. (1997) *J. Vac. Sci. Technol. A* 15: 1704-1709.
30. Klyushin A.Yu., Rocha T.C.R., Hävecker M., Knop-Gericke A., Schlögl R. (2014) *Phys. Chem. Chem. Phys.* 16 : 7881-7886.
31. Tandon D., Hippo E.J., Marsh H., Sebok E. (1997) *Carbon* 35: 35-44.
32. Citrin P.H, Wertheim G.K., Baer Y. (1978) *Phys. Rev. Lett.* 41: 1425-1428
33. Heimann P., van der Veen J.F., Eastman D.E. (1981) *Solid State Commun.* 38: 595-598.
34. Schaefer A., Ragazzon D., Wittstock A., Walle L.E., Borg A., Bäumer M., Sandell A. (2012) *J. Phys. Chem C* 116: 4564-4571.
35. Weststrate C.J., Lundgren E., Andersen J.N., Rienks E.D.L., Gluhoi A.C., Bakker J.W., Groot I.M.N., Nieuwenhuys B.E. (2009) *Surf. Sci.*, 603: 2152–2157.
36. Saliba N., Parker D.H., Koel B.E. (1998) *Surf. Sci.* 410: 270–282.

37. Min B.K., Alemozafar A.R., Biener M.M., Biener J., Friend C.M. (2005) *Top. Catal.* 36: 77-90.
38. Klyushin A.Yu., Greiner M.T., Huang X., Lunkenbein T., Li X., Timpe O., Friedrich M., Hävecker M., Knop-Gericke A., Schlögl R. *ACS catalysis*, submitted.

Supported information.

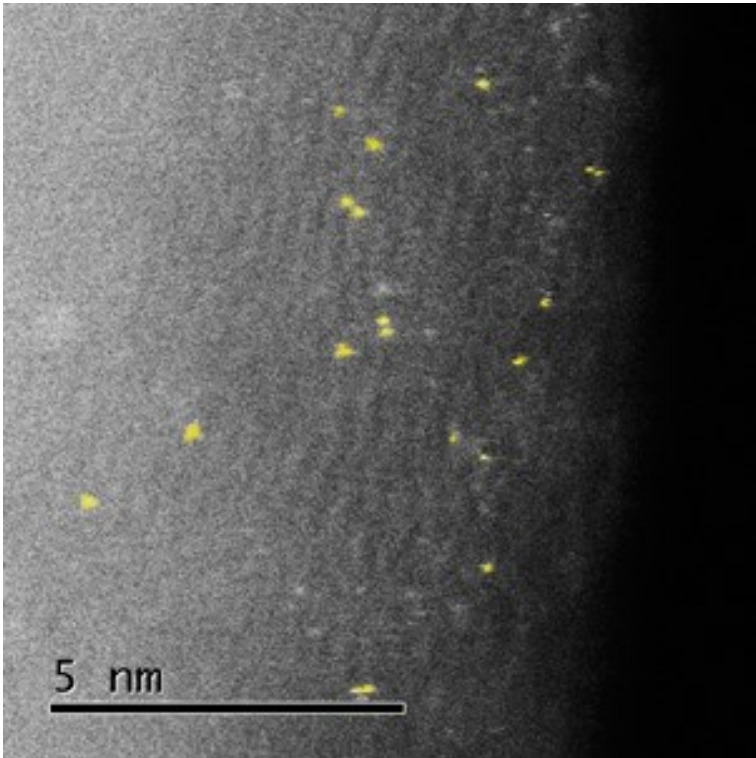


Figure S1. STEM image of fresh Au/N-CNTs. Au NPs are colorized in order to highlight the difference between N-CNTs and Au.

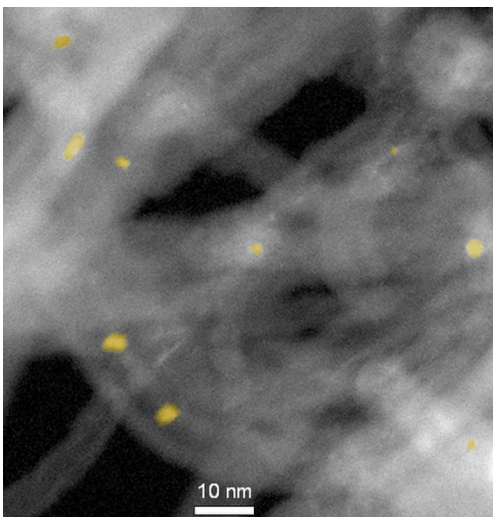


Figure S2. STEM images of fresh Au/O-CNTs. Au NPs are colorized in order to highlight the difference between O-CNTs and Au.

Table S1: Fitting parameters of Au $4f_{7/2}$ spectra of Au/Au foil.

| Au 4f _{7/2} | | | | | | | | |
|-------------------------------------|------------|--------------|------------|--------------|---------------|--------------|------------|--------------|
| | bulk | | surface | | restructuring | | oxide | |
| | BE (eV) | FWHM (eV) | BE (eV) | FWHM (eV) | BE (eV) | FWHM (eV) | BE (eV) | FWHM (eV) |
| UHV | 83.95 | 0.49 | 83.66 | 0.50 | - | - | - | - |
| O ₃ | 83.95 | 0.49 | 83.69 | 0.52 | 83.32 | 0.52 | 85.25 | 1.30 |
| O ₂ after O ₃ | 83.98 | 0.51 | 83.65 | 0.52 | 83.34 | 0.52 | - | - |
| CO+O ₂ | 83.96 | 0.51 | 83.65 | 0.52 | 83.32 | 0.52 | - | - |

Table S2: Fitting parameters of O 1s spectra of Au/Au foil.

| O 1s | | | | | | |
|-------------------------------------|---------------|--------------|---------------|--------------|-----------------------------|--------------|
| | (hydro)carbon | | surface oxide | | Hydroxyl group/contaminants | |
| | BE (eV) | FWHM (eV) | BE (eV) | FWHM (eV) | BE (eV) | FWHM (eV) |
| UHV | 532.50 | 2.06 | - | - | - | - |
| O ₃ | - | - | 529.42 | 1.55 | 531.07 | 1.82 |
| O ₂ after O ₃ | 532.37 | 1.75 | - | - | 530.72 | 1.49 |
| CO+O ₂ | 532.38 | 1.73 | - | - | 530.66 | 1.53 |